Ammonia absorption in ionic liquids-based mixtures in plate heat exchangers studied by a semi-empirical heat and mass transfer framework

Wang, Meng; He, Lijuan; Infante Ferreira, Carlos A.

DOI
10.1016/j.ijheatmasstransfer.2019.02.063

Publication date
2019

Document Version
Final published version

Published in
International Journal of Heat and Mass Transfer

International Journal of Heat and Mass Transfer 134 (2019) 1302–1317

Contents lists available at ScienceDirect

International Journal of Heat and Mass Transfer

journal homepage: www.elsevier.com/locate/ijhmt

Ammonia absorption in ionic liquids-based mixtures in plate heat exchangers studied by a semi-empirical heat and mass transfer framework

Meng Wang [a,*], Lijuan He [b], Carlos A. Infante Ferreira [a]

[a] Process and Energy Department, Delft University of Technology, Leeghwaterstraat 39, 2628 CB Delft, The Netherlands
[b] Department of Environment and Energy, Inner Mongolia University of Science and Technology, China

ARTICLE INFO

Article history:
Received 16 October 2018
Received in revised form 18 January 2019
Accepted 18 February 2019
Available online 28 February 2019

Keywords:
Absorption
Ammonia
Ionic liquid
Lithium nitrate
Plate heat exchanger
Heat transfer
Mass transfer

ABSTRACT

Unfavorable transport properties have always been pointed out as the key factors that hinder the application of ammonia/ionic liquids (NH_3/ILs) in absorption cycles, while heat and mass transfer of these new fluids in components have been rarely reported. In this study, a corrugated plate heat exchanger is selected as the geometry for exploring the absorption of NH_3 in the proposed NH_3/ILs working fluids. The process is studied making use of a semi-empirical framework: experimental data is needed to determine unknown information of heat and mass transfer, and a numerical model is developed making use of frequently applied theories. In addition, relevant transport properties of the NH_3/ILs working fluids are modeled based on collected experimental data. The proposed model is used to study the heat and mass transfer performance during the absorption of NH_3 vapor into NH_3/ILs fluids. Distribution of local parameters and overall heat and mass transfer characteristics are obtained. The performance of absorption of NH_3 into different working fluids is investigated as well. The overall heat transfer coefficient is found around 1.4 kW/(m^2·K) for the most promising working fluid NH_3/[emim][SCN].

1. Introduction

Thermally driven vapor absorption heat pumps and refrigeration systems provide energy-efficient ways of heating and cooling for the industry, agriculture, residential and transport sectors. Recently more and more investigations have been carried out to explore the application of ionic liquids (ILs), a type of room-temperature molten salts, as absorbents in vapor absorption systems. Some ILs have been found with high boiling points, strong affinities with refrigerants and favorable thermal and chemical stabilities. They provide an alternative way to prevent the risks of corrosion and crystallization of H_2O/LiBr pair and weaknesses of low efficiency and complexity of systems with NH_3/H_2O pair. In particular, working pairs of NH_3/ILs have been proposed as working fluids in absorption cycles to remove rectification and distillation sections, and to improve cycles' thermal efficiency. Applications of these fluids used in cycles for heating and cooling introduced in previous studies [54,53] also confirm their promising potentials.

In the past decade, investigations of ILs for applications in absorption cycles were mainly based on thermodynamic analysis for screening suitable working fluids [58]. Recent studied refrigerants with ILs include water [19,1], hydrofluorocarbon [43,6], carbon dioxide [12] and ammonia [56,57]. In these analyses, only thermodynamic properties, for instance the vapor-liquid equilibria, enthalpies and densities, are sufficient. Besides, limited experimental work to evaluate the practical performance on a systematic level was also reported [55,30,34].

Currently, the number of reported studies about the heat and mass transfer processes of IL-based fluids is limited. However these processes are important in sizing the systems in practice. Boman et al. [10] examined plenty of refrigerant/ILs fluids making use of a general heat transfer evaluation. Vertical, flat plate, falling-film heat exchangers were proposed to be used as the main heat and mass transfer components. Wang and Infante Ferreira [54] proposed using plate heat exchangers (PHXs) as absorber, generator, evaporator, condenser and solution heat exchanger in an NH_3/IL single-effect absorption heat pump, considering their compact sizes and superior performance of heat and mass transfer. Brief estimations of sizes and costs of the devices, and of charge of working fluids were carried out based on selected heat transfer correlations. For other application, Wadekar [51] simulated the heat transfer behavior of pure IL, [bmim][Tf_2N], as a heat transfer fluid in different heat exchangers including PHX.

* Corresponding author.
E-mail address: M.Wang-2020@outlook.com (M. Wang).

https://doi.org/10.1016/j.ijheatmasstransfer.2019.02.063
0017-9310/

Nomenclature

A	area [m^2]
c	molar concentration [kmol/m^3]
c_p	heat capacity [J/(kg·K)]
D	mass diffusivity [m^2/s]
d	diameter [m]
F	objective function [–]
$\dot{G}$	mass flux [kg/(m^2·s)]
g	gravitational acceleration [9.8 m/s^2]
$h/\hat{h}$	specific enthalpy/NH_3 component partial enthalpy [J/kg]
L	length [m]
$LMTD$	logarithmic mean temperature difference [K]
M	A general representation of thermophysical properties [–]
M_w	molecular weight [kg/kmol]
$\dot{m}$	mass flow rate [kg/s]
P	pressure [kPa]
$\dot{Q}$	heat flow [kW]
q	vapor quality [kg/kg]
R	radius of the spherical particle [m]
r	correlation coefficient [–]
$T/\Delta T$	temperature (difference) [°C/K]
U	overall heat transfer coefficient [W/(m^2·K)]
$v/\bar{v}$	velocity/average velocity [m/s]
w	mass fraction [kg/kg]
x	molar fraction [mol/mol]

Greek letter

α	heat transfer coefficient [W/(m^2·K)]
β	mass transfer coefficient [m/s]
δ	thickness [m]
ϵ	void-fraction [m^3/m^3]
κ	Boltzmann constant [$1.38064852 \times 10^{-23}$ J/K]
Λ	correction factor of fluid property [–]
λ	thermal conductivity [W/(m·K)]
μ	viscosity [Pa·s]
ρ	density [kg/m^3]
σ	surface tension [N/m]
ξ	frictional factor [–]

Subscript and superscript

1, 2	inlet/outlet of control volumes
A, B	components A and B
abs	absorber
ave	average
c	characteristic (length)
con	condenser
cw	cooling water
eva	evaporator
exp	experiment
f	film
g	(plates) gap
gen	generator
H_2O	H_2O
h	hydraulic (diameter)
in	inlet
ini	initial
int	interface
is	ideal solution
L	liquid
mt	mass transfer
NH_3	species of NH_3
ori	orifice
out	outlet
sat	saturated state
sol	solution
sim	simulation
sub	subcooling state
V	vapor
w	wall

Dimensionless numbers

$Fr = \frac{v_V}{\sqrt{gL_c(\rho_L/\rho_V - 1)}}$	Froude number
$Nu = \frac{\alpha L_c}{\lambda}$	Nusselt number
$Pr = \frac{c_p \mu}{\lambda}$	Prandtl number
$Re = \frac{\rho v L_c}{\mu}$	Reynolds number
$Sc = \frac{\mu}{\rho D}$	Schmidt number
$Sh = \frac{\beta L_c}{D}$	Sherwood number

Abbreviations

ARD	average relative deviation
EXP	experiment
IL	ionic liquid
PHX	plate heat exchanger
RD	relative deviation
SIM	simulation
VLE	vapor-liquid equilibrium/vapor-liquid equilibria
[bmim][BF_4]	1-butyl-3-methylimidazolium tetrafluoroborate
[emim][Tf_2N]	1-ethyl-3-methylimidazolium bis(trifluoromethyl-sulfonyl) imide
[emim][SCN]	1-ethyl-3-methylimidazolium thiocyanate

Studies containing mass transfer for the ILs-based working fluids are even fewer. Meyer et al. [35,36] made use of the analytical functions to describe the combined heat and mass transfer of working fluids ethanol/[emim][DEP] inside the absorber and generator, for which horizontal shell-and-tube heat exchangers were used. Because of the large areas required for the solution heat exchanger, a PHX was implemented. Besides, work on measuring absorption/desorption kinetics and key transport properties, such as mass diffusivity, was also reported for the application of absorption refrigeration cycles, for instance by Bedia et al. [7], Ariyadi and Coronas [5], Ariyadi et al. [4] and Chen et al. [17].

Previous work demonstrated that PHX can be a promising heat and mass exchanger in the IL-based absorption systems. A recent operation of absorption heat transformer using H_2O/[emim][OMs] fluids reported by Merkel et al. [34] brought this idea into practice. They implemented PHXs as evaporator, condenser and solution heat exchanger, a modified PHX with a liquid distributor was used as absorber. However, the heat and mass transfer performance of the IL-based working fluids inside plate heat exchangers was not studied in a detailed way.

On the other hand, plate heat exchangers have been frequently studied for NH_3 absorption systems. Kang et al. [29] compared the NH_3/H_2O absorption inside PHX with two different modes: falling film absorption and bubble absorption, with a control volume analysis. Cerezo et al. [16] reported an experimental study of an NH_3/H_2O bubble absorber using a PHX. A comparison with a numerical model was also presented in the work of Cerezo et al. [14]. Cerezo et al. [15] compared the performance of the bubble absorber using a PHX for the working fluids NH_3/H_2O, $NH_3/LiNO_3$ and NH_3/NaSCN with a similar numerical model previously introduced and con-

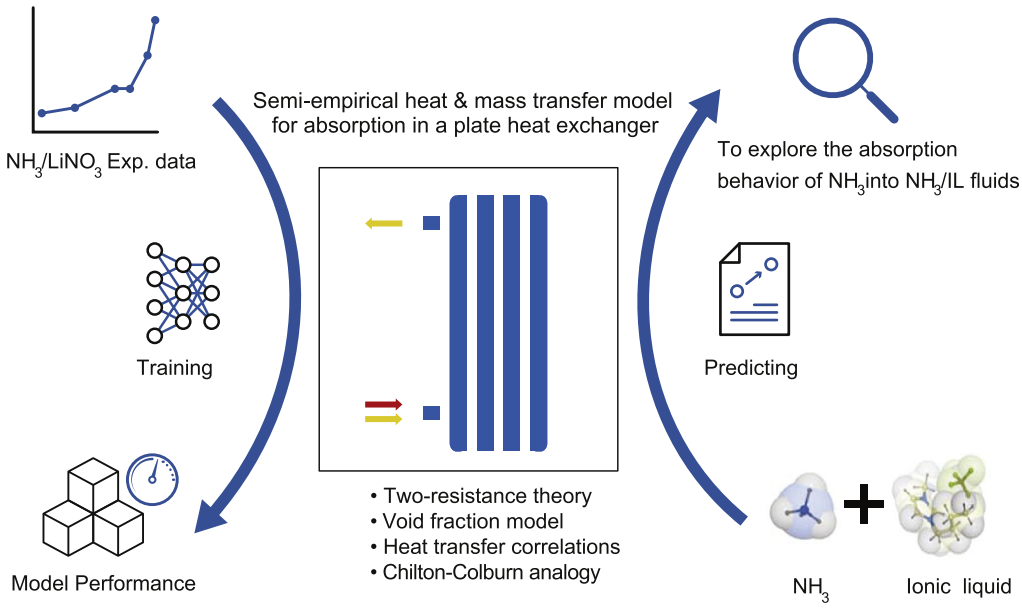

Fig. 1. Outline of this study.

cluded that the $NH_3/LiNO_3$'s high viscosity weakens its performance in the absorber. Experimental work was then carried out to compare the effect of adding H_2O into $NH_3/LiNO_3$ in a PHX used as a bubble absorber by Oronel et al. [41]. Recently Triché et al. [48] presented an experimental and numerical study of heat and mass transfer in a falling film absorber with the fluids NH_3/H_2O. Tao et al. [44] reviewed work on two-phase downward flow within PHX and proposed flow pattern maps. These maps are instructive to distinguish different mechanisms of NH_3 absorption or condensation in the PHX.

The literature review indicates that heat and mass transfer research regarding NH_3/IL working fluids has not been reported yet. In this study, a numerical study about heat and mass transfer during absorption of NH_3 into NH_3/IL solution will be carried out. A corrugated PHX is selected as the geometry of the absorber. The outline of this study is illustrated in Fig. 1.

A semi-empirical model is proposed to describe the heat and mass transfer performance of the vapor absorption inside PHX. The model is called "semi-empirical" because parts of it are based on frequently applied theories, such as the two-resistance theory with a gas-liquid interface; void-fraction for a prediction of the liquid film thickness; and Chilton-Colburn analogy to couple the heat and mass transfer. On the other hand, undetermined parameters describing the heat and mass transfer characteristics are obtained from a similar experimental investigation - NH_3 absorption by $NH_3/LiNO_3$ fluids. Also, relevant thermodynamic and transport properties of the studied NH_3/IL fluids are modeled based on the collected experiment data. With these thermophysical properties, heat and mass transfer performances are investigated during NH_3 absorption by different NH_3/ILs fluids inside the PHX.

2. Heat and mass transfer framework for the vapor absorber

2.1. General description

In the working fluid side of the PHX absorber, there are two different flow regimes considered in this study: the two-phase vapor-liquid flow and the single-phase subcooled liquid flow. The model of the subcooled single-phase flow (only heat transfer occurs) can be derived from the other one, thus here only the modeling of the two-phase vapor-liquid flow is introduced.

As shown in Fig. 2, taking advantage of the symmetry feature of the plate heat exchanger, only a plate with its surrounding two streams are studied in this model. Distribution of parameters is considered by numerically dividing the plate heat exchanger into small control volumes along the bulk streams (the length of the plates). The heat and mass transfer of the three flow streams, i.e., the cooling water, the solution and the NH_3 vapor, are studied in each control volume. Regarding the vapor absorption, the two-resistance theory with an interface is applied to describe the heat and mass transport between the vapor-liquid interface with its surroundings (the vapor and solution bulk streams, respectively). Heat and mass transfer fluxes are calculated using empirical correlations. This modeling method has been successfully adopted to investigate overall two-phase heat and mass transfer processes with complex geometrical structures in previously studies [14,28,48].

These general simplifications are adopted to develop the heat and mass transfer model of absorption:

- Absorption is assumed at a steady state.
- The liquid film is assumed to have a symmetrical thin feature contacting with plates.
- Interface is in equilibrium at saturated conditions.
- The distribution along the width of plates is taken as uniform.
- Properties and conditions at the inlet of a control volume are used to represent the local ones.
- Absorbents are regarded as non-volatile, thus no mass transfer of it occurs in the vapor phase.
- Thermal boundary layers between the two-phase and single-phase regions show a smooth transition.
- Heat conduction along the thickness of plates is negligible.
- Longitudinal conduction of plates and fluids are negligible.
- No heat loss to the environment.

The implementation of the calculation is shown in Fig. 3. In this study, the calculation is carried out from the bottom of the plate heat exchanger to its top. Control volumes are discretized according to their lengths, which are identical in the current setting. For each control volume, conditions (flow, temperature, pressure and composition) in the bottom are taken as the input. Sub-routines for obtaining other thermophysical properties, film thicknesses

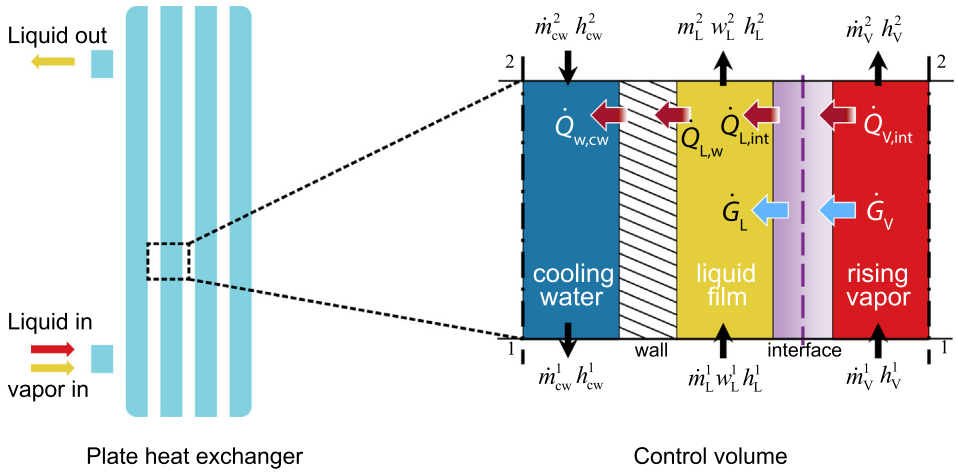

Fig. 2. Schematic representation of the modeled absorber (left), and the split control volume (right). The corrugated surface of plates is not shown.

and dimensionless numbers are used before starting the conservation calculations. An iteration is carried out based on the heat and mass balances to obtain the interface temperature, T_{int}.

Calculated results are heat and mass transfer properties and the outlet parameters. The latter ones will be used as the input for the next control volume. For the studied cases, 400 uniform control volumes are used after a grid dependency evaluation.

2.2. Film thickness

Symmetrical thin films on plates can be used to represent the liquid flow of various flow patterns, such as film and slug flow, for vapor-liquid two phase flow in PHXs. In this study, the solution streams are also simplified as liquid films. The simplification is verified in the last section of this study.

The thickness of the liquid film is obtained with the help of the void-fraction. NH_3 vapor is assumed surrounded with liquid films between plates, as shown in Fig. 2. Void-fraction is applied to estimate the fraction of the channel cross-sectional area that is occupied by the gas phase. With it, the film thickness is expressed as,

$$\delta_f = (1-\epsilon)\frac{L_g}{2} \tag{1}$$

where L_g is the gap between plates.

The void-fraction, ϵ, is obtained according to the frequently used Eq. (2), which has been proposed by Zivi et al. [59] based on the principle of minimum entropy production for annular two-phase flow:

$$\frac{1}{\epsilon} = 1 + \left(\frac{1-q}{q}\right)\left(\frac{\rho_V}{\rho_L}\right)^{2/3} \tag{2}$$

One of the advantages of applying the void-fraction to predict the film thickness is that the thickness is related with the vapor quality (q), ensuring that the thickness turns to the gap dimension when vapor is fully absorbed.

2.3. Pressure drop

The frictional pressure drop of a stream along a channel is estimated using Eq. (3):

$$\frac{dP}{dL} = \xi\frac{\rho\bar{v}^2}{2d_h} \tag{3}$$

where $d_h = 2L_g$.

For the plate heat exchanger, the friction factor, ξ, is obtained from the experimental data of Amaris Castilla [3].

2.4. Heat transfer

The heat transfer characteristics of the two single-phase flows: cooling water, and NH_3 vapor (heat transfer to the interface), are described using correlations as summarized in Table 1.

Characteristic lengths of dimensionless numbers are the hydraulic diameters for both cases.

Previous work conducted by peers distinguished the heat transfer between liquid film bulk and the wall with that between the interface and the film bulk [48,37]. Analytic work by Grossman [24] and Brauner [11] also confirms the need of separately considering the two heat transfer layers within liquid films.

However, the thin feature of the film makes its heat transfer characteristic more difficult to describe than other streams. Additionally, the interface which is introduced for a convenience to study absorption problems does not naturally exist. The heat and mass transfer related to it cannot be practically detected. In this work, with the help of the proposed model, the Nusselt numbers of the liquid film, $Nu_{L,w}$ and $Nu_{L,int}$, will be determined using the experimental data by Amaris Castilla [3].

The heat transfer of the solution stream to the wall should smoothly go from the vapor-liquid two-phase region to the single-phase one. Considering this natural fact, the heat transfer of solution to the wall in the two-phase region and that in the single-phase region should have comparable characteristics. This is realized by assuming the heat transfer boundary layers share the same thicknesses in the two consecutive control volumes during the regime transition.

2.5. Mass transfer

For the studied problem with absorption controlled by the liquid phase, the only mass transfer takes place from the interface to the solution bulk stream. The Chilton-Colburn analogy is applied to obtain the mass transfer coefficient between them, which is based on the boundary layers analogy.

The analogy is expressed simply for heat and mass transfer as,

$$\frac{Sh}{Nu_{L,int}} \approx \left(\frac{Sc}{Pr}\right)^{1/3} \tag{4}$$

The characteristic lengths of the dimensionless numbers for the liquid film in the two-phase region are selected as the film thickness.

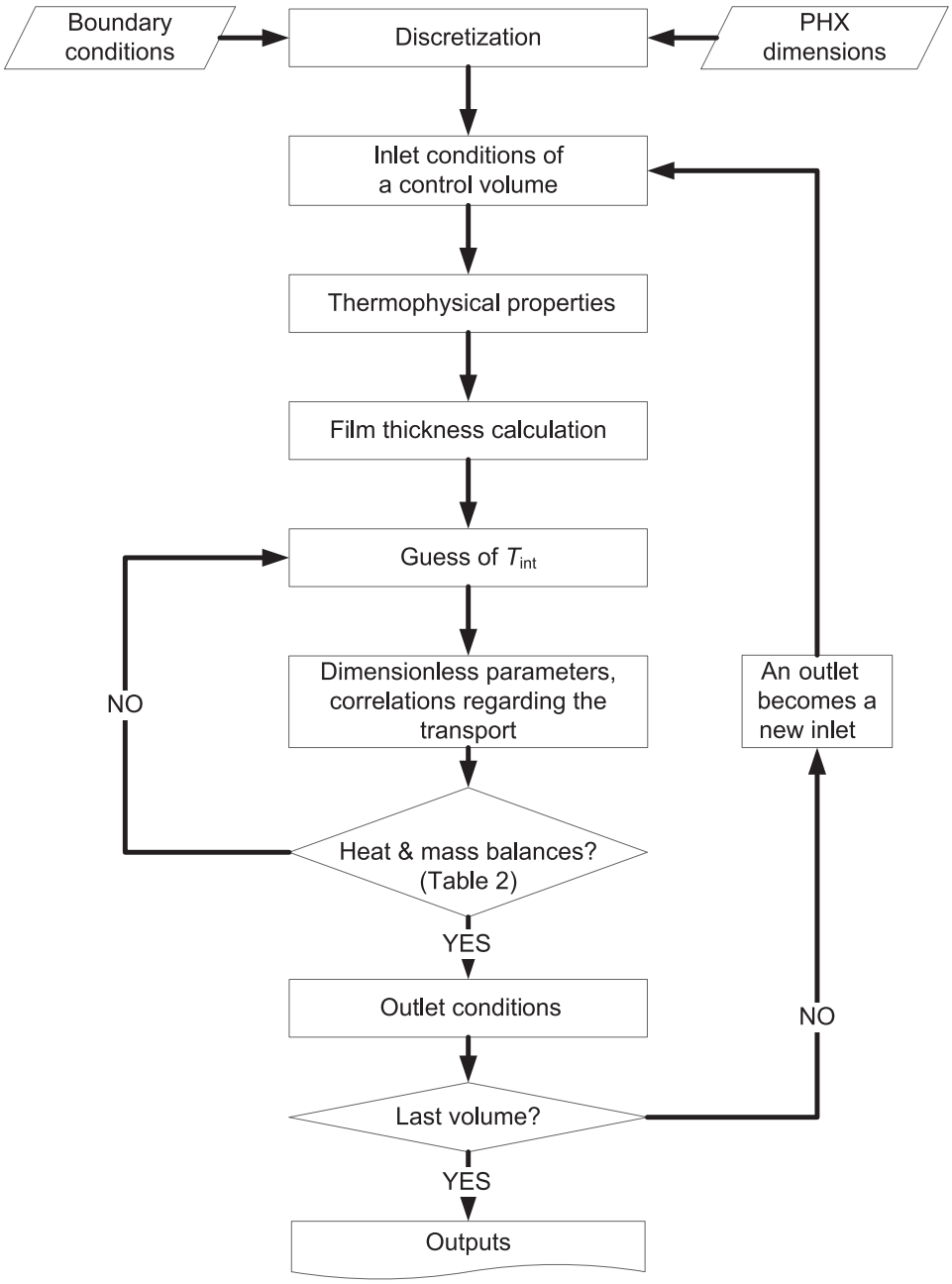

Fig. 3. Calculation procedure of the model: A set of transport conservation equations are carried out in each discretized control volume. Sub-routines regarding the thermophysical properties, film thicknesses and dimensionless numbers are implemented. An iteration is carried out to obtain the interface temperature based on the heat and mass transport conservation equations. The outlet of each volume is used as the input to the next one.

Table 1
Correlations of heat transfers used in this study.

	Cooling water	Vapor with the interface
Correlation	$Nu = 0.858Re^{0.555}Pr^{1/3}$	$Nu = 8.23$
Source	Amaris Castilla [3]	Bergman et al. [8]

2.6. Transport conservation equations

The heat and mass transport conservation equations of the liquid-vapor two-phase flow during absorption are listed in Table 2.

Regarding these equations, parameters with superscripts are inputs or outputs of a calculation: "1" denotes the input in the bottom of a control volume, and "2" denotes the output on top.

The amount of unknown parameters and that of the equations equals with each other, indicating the problem is solvable. For an easy solving, an iteration of the unknown interface temperature, T_{int}, is conducted until the assumed value guarantees that the heat and mass balances of the control volume are satisfied.

3. Parameters determination and model performance

Amaris Castilla [3] experimentally investigated the absorption of NH_3 in an $NH_3/LiNO_3$ solution inside a plate heat exchanger. The working fluids flow from the bottom of the PHX to its top in a counter-current direction with the cooling water stream, which is identical with the studied problem. The geometrical parameters of the tested PHX are listed in Table 3.

The required properties of fluid $NH_3/LiNO_3$, are listed in Table 4 with their sources.

Table 2
Transport conservation equations describing the absorber section with two-phase flow.

	Equations
Energy balance of the cooling water stream	$\dot{Q}_{w,cw} - \dot{m}^1_{cw}h^1_{cw} + \dot{m}^1_{cw}h^2_{cw} = 0$
Energy balance of the solution stream	$\dot{G}_{int}\hat{h}_L + \dot{Q}_{int,L} - \dot{Q}_{L,w} + \dot{m}^1_L h^1_L - \dot{m}^2_L h^2_L = 0$
Energy balance of the vapor stream	$-\dot{G}_{int}\hat{h}_V - \dot{Q}_{V,int} + \dot{m}^1_V h^1_V - \dot{m}^2_V h^2_V = 0$
Energy balance through the wall	$\dot{Q}_{L,w} = \dot{Q}_{w,cw}$ $\dot{Q}_{w,cw} = \alpha_{w,cw}\left(T_w - T^1_{cw}\right)A_{int}$ $\dot{Q}_{L,w} = \alpha_{L,w}\left(T^1_L - T_w\right)A_{int}$
Energy balance through the interface	$\dot{G}_{int}A_{int}\hat{h}_V + \dot{Q}_{V,int} = \dot{G}_{int}A_{int}\hat{h}_L + \dot{Q}_{int,L}$ $\dot{Q}_{int,L} = \alpha_{int,L}\left(T_{int} - T^1_L\right)A_{int}$ $\dot{Q}_{int,V} = \alpha_{int,V}\left(T^1_V - T_{int}\right)A_{int}$
Mass balance of the solution stream	$\dot{G}_{int}A_{int} + \dot{m}^1_L - \dot{m}^2_L = 0$ $\dot{G}_{int} = M_w\beta(c_{int} - c_L)$
Mass balance of the vapor stream	$-\dot{G}_{int}A_{int} + \dot{m}^1_V - \dot{m}^2_V = 0$
NH_3 species balance in the liquid stream	$\dot{G}_{int}A_{int} + \dot{m}^1_L w^1 - \dot{m}^2_L w^2 = 0$

Table 3
The geometrical parameters of the studied PHX.

Length	[m]	0.53
Width	[m]	0.112
Amount of channels	[–]	3
Space between plates	[m]	0.002
Total heat transfer area	[m^2]	0.1

Table 4
Thermo-physical properties of $NH_3/LiNO_3$ studied in this work.

	Property	Source
ρ	Density	Infante Ferreira [26]
P-T-w	Vapor-liquid equilibrium	Libotean et al. [33]
c_p	Heat capacity	Infante Ferreira [26]
h	Enthalpy	Infante Ferreira [26]
μ	Viscosity	Libotean et al. [32]
λ	Thermal conductivity	Cuenca et al. [18]
D	Mass diffusivity	Venegas et al. [50]
σ	Surface tension	Venegas et al. [50]

3.1. Parameters determination

In the proposed framework described in Section 2, determination of the performance of the absorber requires the friction factors and heat and mass transfer coefficients for the liquid film. 14 sets of experimental data at different solution flow conditions, as shown in Table 5, are used to obtain the unknown parameters in the proposed heat and mass transfer framework: Nu numbers of the liquid film and the frictional factor. Correlations of these parameters with solution flows are also presented.

Firstly, to obtain the friction factor, ξ, data of inlet and outlet pressures in the working fluids side are used with Eq. (3). The values of ξ from 14 independent cases present a relation to the solution Re_L at the entrance, which is based on the hydraulic diameter of the PHX (d_h), as shown in Fig. 4.

The inlet conditions of solution, vapor and cooling water streams are used as inputs in the proposed heat and mass transfer model. Since the cooling water enters at the top of the absorber, the value of outlet temperature needs to be iterated. With the heat transfer area specified, the heat duty and temperature distributions are the calculation results.

To find the suitable $Nu_{L,w}$ and $Nu_{L,int}$ to be used in the model to describe the absorption problem, optimizations are carried out based on the 14 experimental cases.

For each experimental case from Amaris Castilla [3], an optimization work is conducted in which the two Nu numbers have been optimized. The objective function of the optimization is the minimization of the following function,

$$F = \sqrt{\left[\frac{\left(\dot{Q}/A\right)_{exp} - \left(\dot{Q}/A\right)_{sim}}{\left(\dot{Q}/A\right)_{exp}}\right]^2} + \sqrt{\left[\frac{(U)_{exp} - (U)_{sim}}{(U)_{exp}}\right]^2} \quad (5)$$

Beside using heat flux, $\dot{Q}/A$, as an indication to ensure the energy balance, the overall heat transfer coefficient, U, is applied to take into account the heat transfer performance. Both the mean square deviations of them have been considered so that the effect of different temperature driving forces is taken into account. For each experimental case, implementation in the model of the obtained Nu numbers results in an accurate prediction of the system performance.

The optimization and correlation procedures are illustrated in Fig. 5.

The values of $Nu_{L,w}$ and $Nu_{L,int}$ from the 14 independent optimizations are presented in Table 6 and Fig. 6. The comparison of

Table 5
Experimental data used to obtain unknown parameters in the proposed heat and mass transfer framework and the performance of parameters determination.

Case	$\dot{m}^{in}_L$	T^{in}_L	w^{in}_L	$\dot{m}^{in}_V$	P^{in}_L	P^{out}_L	$\dot{m}^{in}_{cw}$	T^{in}_{cw}	$\dot{Q}/A$ [kW/m^2]			U [W/(m^2·K)]		
	[kg/h]	[°C]	[–]	[kg/h]	[kPa]	[kPa]	[kg/h]	[°C]	EXP	SIM	RD [–]	EXP	SIM	RD [–]
1	10.39	44.93	0.4524	1.56	521.24	516.06	271.54	37.48	4.84	4.82	−0.003	1512.1	1504.7	−0.005
2	15.38	45.70	0.4500	1.88	513.86	507.94	270.66	38.23	6.97	7.00	0.004	1585.3	1606.9	0.014
3	20.45	45.63	0.4538	1.93	516.14	509.3	264.19	38.14	8.12	8.13	0.002	1800.4	1803.9	0.002
4	25.34	45.69	0.4497	2.20	510.34	502.24	267.19	38.63	9.69	9.49	−0.020	1867.9	1896.1	0.015
5	40.24	44.71	0.4528	2.80	517.38	505.08	275.38	38.80	12.18	12.19	0.001	2242.4	2383.1	0.063
6	30.88	45.64	0.4526	2.09	519.63	510.55	266.64	38.98	10.47	9.55	−0.088	2042.0	2303.2	0.128
7	50.01	46.15	0.4533	2.54	509.85	495.5	266.13	39.61	13.08	12.27	−0.062	2246.4	2471.9	0.100
8	10.57	45.39	0.4519	1.34	521.39	516.67	266.62	41.46	3.38	3.38	0.000	1531.9	1532.0	0.000
9	15.33	45.39	0.4530	1.01	514.77	509.4	268.39	41.73	4.34	4.03	−0.072	1772.2	1724.3	−0.027
10	20.55	45.85	0.4528	1.25	515.8	509.62	267.93	41.92	5.3	5.12	−0.035	1846.8	1871.9	0.014
11	25.33	46.10	0.4523	1.52	518.95	511.82	267.62	42.18	6.08	6.07	−0.001	1977.7	1991.9	0.007
12	30.25	45.00	0.4527	1.65	518.21	509.97	267.09	42.25	6.25	6.25	0.000	2406.5	2566.7	0.067
13	48.85	45.87	0.4518	1.45	513.26	501.43	269.16	43.23	7.56	6.57	−0.131	2707.6	3182.8	0.176
14	40.59	45.32	0.4496	1.74	515.08	504.69	269.02	42.68	7.08	7.09	0.001	2535.7	2545.0	0.004

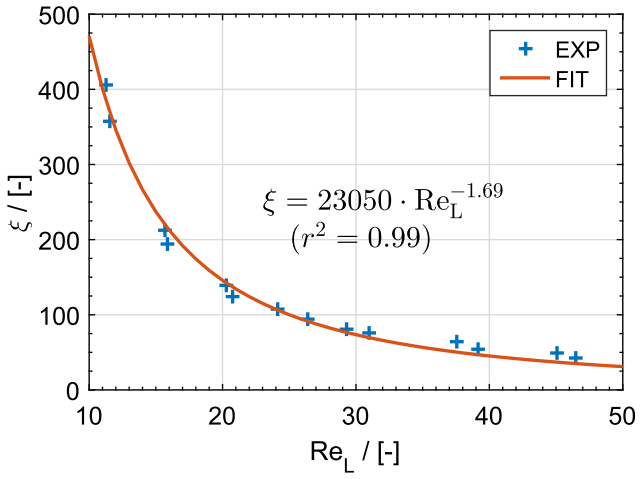

Fig. 4. Values of frictional factor, ξ, of the experimental cases with their correlations to Re_L.

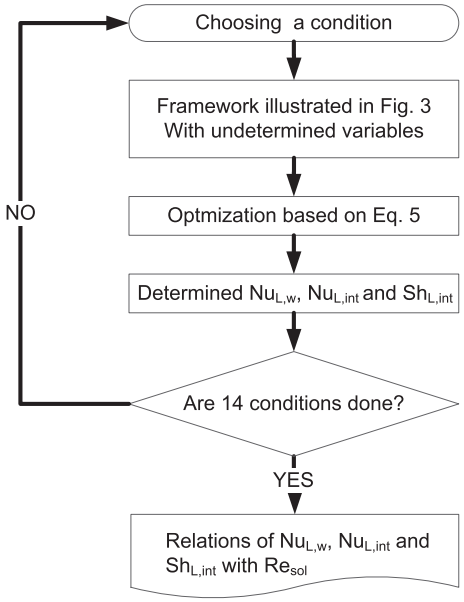

Fig. 5. Steps to determine unknown heat and mass transfer characteristics and their relations with flow rates.

Table 6
Determined Nusselt numbers of liquid film from experimental data.

Case	Re_L^{in}	$Nu_{L,w}$	$Nu_{L,int}$
1	11.27	2.49	17.60
2	15.72	2.25	46.25
3	20.33	3.65	50.20
4	24.13	3.41	67.08
5	37.60	4.53	85.95
6	29.29	4.94	55.64
7	45.05	5.32	93.50
8	11.58	1.61	17.82
9	15.89	3.38	35.06
10	20.75	3.97	43.27
11	26.35	3.90	52.62
12	31.03	4.86	47.30
13	46.48	5.87	78.06
14	39.17	4.42	70.93

optimized results of $\dot{Q}/A$ and U with the experimental ones is listed in Table 5. The deviations are acceptable at an overall device level.

As shown in Fig. 6, the values of optimized $Nu_{L,w}$ and $Nu_{L,int}$ show clear relations with the liquid Reynolds number. By correlating these data to a frequently used form of $Nu = aRe^bPr^{1/3}$, coefficients can be determined, as shown in Fig. 6.

To confirm the validity of the correlations, the additional 16 independent experiments also reported by Amaris Castilla [3], which were not used in the generation of the correlations, are used to check the reliability of obtained Nu numbers. The relative deviations between experimental and simulation results for $\dot{Q}/A$ and U are, 5.6% and 1.8% in average. Conditions of these experiments and comparisons of experimental and predicted values are listed in a table provided as supporting information.

The thickness of heat transfer boundary layers can be estimated using $\frac{\delta_f}{Nu_L}$. (Note that the film thickness is used as the characteristic length for the heat and mass transfer of the liquid film.) The obtained Nusselt numbers in this work provide a relation: $\frac{\delta_f}{Nu_{L,w}} + \frac{\delta_f}{Nu_{L,int}} < \delta_f$. It reflects the heat transfer on the liquid film is not only dominated by conduction within a heat transfer boundary layer. The additional convection effects on the heat transfer can be enhanced by the corrugated plates surface and the coupled mass transfer.

3.2. Model performance

The proposed model is capable of capturing variable distributions, for instance for temperatures and NH_3 mass fractions as shown in Fig. 7, for a typical absorption case.

For the working fluids side, temperature of NH_3 vapor increases rapidly at the beginning of the absorption. Then it reaches a peak which is at a comparable level with the local temperature of the solution, and drops until it is completely absorbed.

The curve of solution temperature shows a trend with three obvious sections. It firstly raises at the entrance of the absorber, and then decreases moderately until the vapor absorption completes. After that, the temperature drops more rapidly. For convenience, as divided by the vertical dashed lines, the three sections are named as entrance of absorption, absorption and non-absorption regions.

The temperature of interface is close to that of the liquid, since the heat resistance between interface and liquid film is small. On the other hand, the NH_3 fraction difference between them is larger at the entrance. It drives a high rate of NH_3 mass transfer from the interface to the liquid. The large transfer of mass also leads to the release of a large amount of absorption heat, which in turn increases the liquid temperature. An increase of interface temperature causes the equilibrium fraction of NH_3 to drop, leading to a reduction of the absorption rate. In the no-absorption region, since no absorption heat is released, the solution temperature drops sharply.

4. Thermophysical properties of studied ammonia/ionic liquids fluids

The properties of pure ammonia are from NIST database refprop 9.1 [31].

The three ionic liquids under consideration for the ammonia absorption are the ones investigated in the authors' previous work [53]: 1-butyl-3-methylimidazolium tetrafluoroborate ([bmim][BF_4], CAS registry No.174501-65-6), 1-ethyl-3-methylimidazolium thiocyanate ([emim][SCN], CAS registry No.331717-63-6) and 1-ethyl-3-methylimidazolium bis(trifluo-

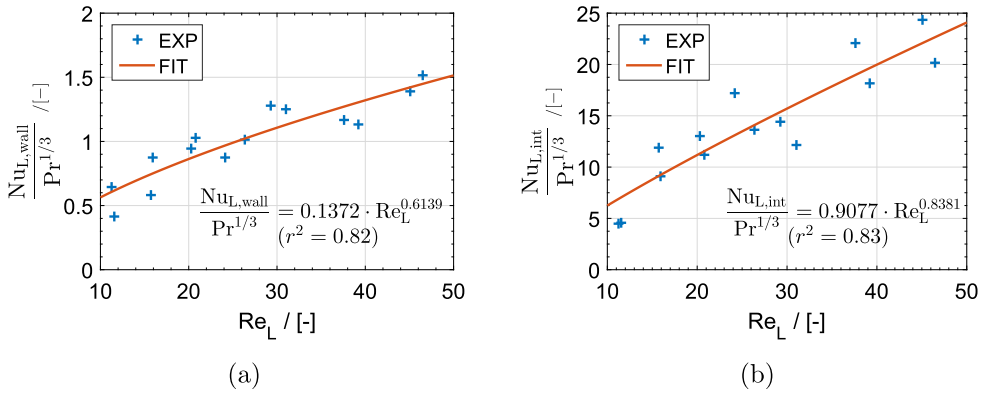

Fig. 6. Results of the independently optimized Nusselt numbers of the solution film with their correlations to the solution Reynolds numbers. (a) Nusselt numbers of the solution film to the wall; (b) Nusselt numbers of the solution film to the interface.

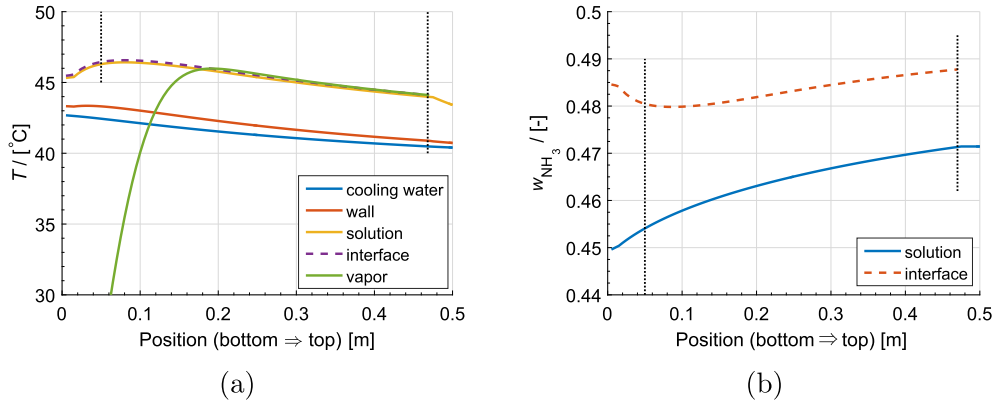

Fig. 7. Distributions of (a) temperature, and (b) NH_3 mass fraction of the experimental absorption Case 14 (Table 5).

romethylsulfonyl) imide ([emim][Tf_2N], CAS registry No.174899-82-2).

Vapor-liquid equilibrium (VLE) properties, densities, heat capacities and enthalpies of the studied ILs and their NH_3 mixtures, and the relevant modeling methods have been reported in the authors' previous work [54,52,53]. In this section, only the relevant transport properties of the studied working fluids are introduced, for length and simplicity reasons.

For the pure ILs, the correlations for their relevant experimental properties are summarized in Fig. 8 and Table 7.

4.1. Viscosity

High viscosity is always mentioned as the main weakness which prevents applications of the ILs in absorption systems. Reported viscosity data of pure [emim][SCN] [20], [bmim][BF_4] [42] and [emim][Tf_2N] [25] are plotted in Fig. 8(a).

Three-parameter Vogel equations are used to correlate these viscosity data, which are shown in Table 7. The viscosity of [bmim][BF_4] is larger than the one of the other two ILs. This will lead to a negative influence on its heat transfer performance.

Previously reported viscosity data of NH_3/IL solutions measured by Cera-Manjarres [13] indicate that adding NH_3 reduces the viscosity of the mixture. Even though viscosities of solutions containing NH_3 and the considered three ILs have not been reported yet, Eq. (6) is used in this study. The excess term is neglected here, which has been discussed in literature, for instance in the work of Gao and Wagner [22].

$$\ln \mu_{is} = x_A \ln \mu_A + x_B \ln \mu_B \tag{6}$$

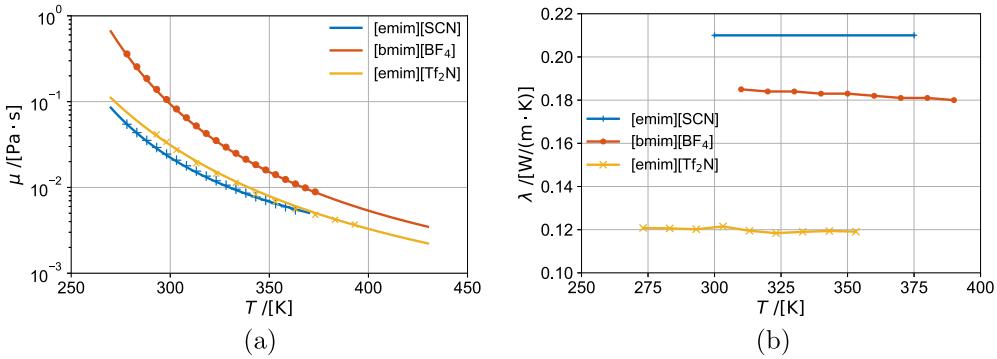

Fig. 8. Experimental data and trends (Table 7) of (a) viscosities [20,42,25] and (b) thermal conductivities [46,49,21] of the three studied ILs.

Table 7
Molecular weights and correlations of relevant thermo-physical properties for the three investigated ILs.[a]

	[emim][SCN]	[bmim][BF_4]	[emim][Tf_2N]
Mw [kg/kmol]	169.25	226.02	391.31
μ [Pa·s]	$\ln\mu = -7.839 + \frac{486}{T-179.6}$	$\ln\mu = -8.99 + \frac{871.1}{T-168.4}$	$\ln\mu = -9.717 + \frac{1111}{T-122.2}$
λ [W/(m·K)]	0.21	0.183	0.12
σ [N/m]	$\sigma = 7.926\times10^{-2} - 8.709\times10^{-5}\times T$	$\sigma = 6.031\times10^{-2} - 5.639\times10^{-5}\times T$	$\sigma = 5.114\times10^{-2} - 5.145\times10^{-5}\times T$
D_{NH_3} [m^2/s]	-	$D_{NH_3} = -1.502\times10^{-8} + 5.2\times10^{-11}\times T$	–

[a] T in K.

The deviation of solution viscosities predicted with Eq. (6) in relation to their real values has also been checked using the reported viscosities of 6 NH_3/IL mixtures by Cera-Manjarres [13], as listed in Table 8. Neglecting the excess viscosity term may introduce at worst over −90% deviations (which are underestimated of real values), nevertheless it is still the best one compared with other weight-average methods (mass fraction based, or absolute viscosity based).

4.2. Thermal conductivity

Reported thermal conductivities of pure [emim][SCN] [46], [bmim][BF_4] [49] and [emim][Tf_2N] [21] all indicate almost constant trends in the relevant temperature range as 0.21, 0.183 and 0.12 W/(m·K), respectively (Fig. 8(b)). The thermal conductivities of [emim][SCN] and [bmim][BF_4] are significantly larger than the one of [emim][Tf_2N]. No data for the thermal conductivity of the 3 ILs mixed with NH_3 solutions have been reported in literature. Eq. (7), which is based on weighted average of properties from both components with weights of their mass concentrations, is applied for solutions' thermal conductivities.

$$M_{sol} = w_A M_A + w_B M_B \tag{7}$$

4.3. Surface tension

Surface tensions of pure [emim][SCN], [bmim][BF_4] and [emim][Tf_2N], have been reported respectively by Almeida et al. [2], Ghatee and Zolghadr [23] and Tariq et al. [45]. They show linear trends with the temperature change. For the NH_3/IL mixtures, its values are estimated using the weight-averaged value based on the pure components (Eq. (7)).

4.4. Mass diffusivity

Effective mass diffusivities of NH_3 in [bmim][BF_4] have been reported by Bedia et al. [7] for 3 temperature levels. The values of NH_3 in [emim][Tf_2N] have been reported by Ariyadi et al. [4] for 3 pressure levels at 30 °C.

As a new proposed working fluid for the absorption cycle, the mass diffusivity of NH_3 in [emim][SCN] has not been reported yet. Nevertheless the relation of it with the viscosity can be used for an estimation.

Stokes-Einstein equation provides a relation of the mass diffusivity of a solute A into a stationary component B with the viscosity of component B, which is based on the Nernst-Einstein relation and Stokes' law [9]:

$$\frac{D_{AB}\mu_B}{\kappa T} = \frac{1}{4\pi R_A} \tag{8}$$

where κ is the Boltzmann constant and R_A is the radius of the spherical particle A.

The underlying theory of Stokes-Einstein equation has been developed to a number of empirical correlations, which permits a estimation of diffusivities in terms of more easily measured properties such as viscosity and molar volume. For instance for the IL-based fluids, Morgan et al. [39] proposed correlations for gases in imidazolium-based ILs with a different exponent of the viscosity of ILs ($D_{gas,IL} \propto \mu_{IL}^{-0.6}$). However, these authors did not include NH_3.

In this work, a different dependence is found using the limited mass diffusivity data of NH_3 in ILs reported in the work of Bedia et al. [7] and Ariyadi et al. [4], with the available viscosity data from Salgado et al. [42], Cera-Manjarres [13] and Hofmann et al. [25], for the cases of NH_3 absorption.

The mass diffusivity data of NH_3 with different imidazolium-based ILs are shown in Fig. 9. Data in Fig. 9(a) were measured at different temperature levels, while data in Fig. 9(b) show mass diffusivities at different pressure levels at 30 °C.

As shown in Fig. 9, the mass diffusivity of NH_3 in ILs as a function of the viscosity of ILs presents a slope of −1.45 in loglog diagrams. Therefore, with a known NH_3 mass diffusivity and viscosities of a known IL, the trend can be applied to estimate NH_3 mass diffusivity in the other IL via,

$$D_{NH_3,ILB} = \left(\frac{\mu_{ILB}}{\mu_{ILA}}\right)^{-1.45} \cdot D_{NH_3,ILA} \tag{9}$$

The averaged relative deviations of correlations for the current data are 41.76% and 38.99%, respectively for cases in Fig. 9(a) and (b). Nevertheless, the correlation is simple and clear. The only unknown mass diffusivity is for [emim][SCN] and is obtained using Eq. (9).

Table 8
Deviations of the predicted values of viscosities (by using Eq. (6)) from the real values using the data reported by Cera-Manjarres [13].

Working fluids[a]	ARD	max RD
NH_3/[N112(2OH)][TfO]	−0.450	−0.871
NH_3/[N112(2OH)][NTf_2]	−0.547	−0.917
NH_3/[N111(2OH)][NTf_2]	−0.556	−0.904
NH_3/[N1113][NTf_2]	−0.503	−0.901
NH_3/[EtOHmim][BF_4]	−0.582	−0.964
NH_3/[EtOHmim][NTf_2]	−0.560	−0.917

[a] Nomenclature of ILs is according to the original work of Cera-Manjarres [13].

5. Prediction using the model for ammonia/ionic liquid absorption in PHX

The exploration of heat and mass transfer performance of NH_3/ILs absorption is based on the application of NH_3 absorption heat pumps in an operation condition of $T_{gen}/T_{con}/T_{abs}/T_{eva}$ = 120/45/45/10 °C [54]. Some conditional parameters in the working fluid side can be determined referring to the thermodynamic analysis, such as the circulation ratio (corresponds to the term, $\dot{m}_L^{in}/\dot{m}_V^{in} + 1$), the mass fraction and the temperature in the solution inlet, w_L^{in}, T_L^{in}, the solution outlet temperature, T_L^{out}, and the vapor inlet temperature, T_V^{in}. They are

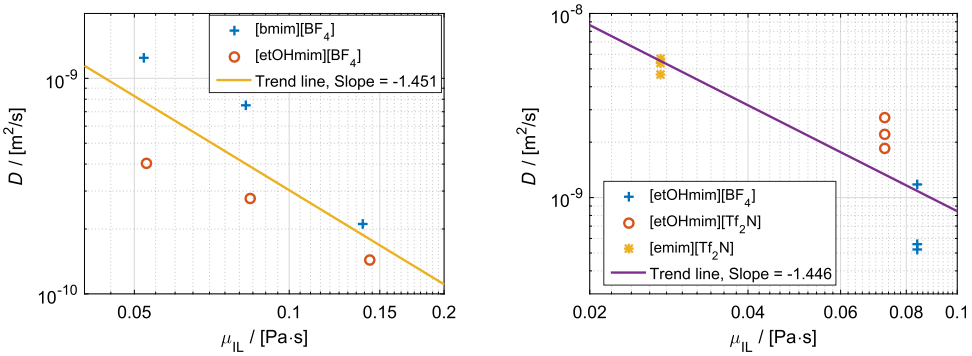

Fig. 9. The relations of effective mass diffusivities of NH_3 in ILs with respect to viscosities of corresponding pure ILs. (a) Effective mass diffusivities at different temperature levels reported by Bedia et al. [7] (ARD of 41.76%); (b) Effective mass diffusivities at different pressure levels reported by Ariyadi et al. [4] (ARD of 38.99%). The information about the ILs shown can be found in the original studies.

part of boundary conditions in the following discussion. Their values for the three studied NH_3/IL working fluids are listed in Table 9.

The heat and mass transfer performance of $NH_3/LiNO_3$ for an absorption heat pump application is also calculated for reference purposes. Following the same method in Wang and Infante Ferreira [54], the circulation ratio and coefficient of performance (for heating) of the $NH_3/LiNO_3$ fluid in absorption heat pumps are found to be 4.64 and 1.63, respectively, at the same operating condition. The boundary conditions of these fluids are listed in Table 9 as well.

The geometrical parameters of the PHX are the same as the ones listed in Table 3. For an easy comparison, the vapor flow and cooling water inlet conditions are kept the same for all cases, which are $\dot{m}_V = 3.89 \times 10^{-4}$ kg/s, $T_{cw}^{in} = 40$ °C and $\dot{m}_{cw} = 1.41 \times 10^{-2}$ kg/s.

5.1. Distributions of parameters

Temperature distributions during absorption of the studied cases are provided in Fig. 10.

As shown in Fig. 10, the temperature distributions along PHXs of two studied ILs cases share similar trend with that found in the experimental cases, except for the case with [bmim][BF_4], see Fig. 7. Three sections are also clearly detected for the temperature distribution of the solution streams. For the reference case (Fig. 10 (d)), the absorption is not finished, thus the single-phase convection region is not there. Compared with the ILs cases, the reference case shows a less rapid increasing of vapor temperature. The temperature rise of the solution stream is more obvious at the entrance.

Table 9
Determined boundary conditions in the NH_3/IL working fluids side of the absorber, for an absorption heat pump application.[a]

Working fluid	$\dot{m}_L^{in}/\dot{m}_V^{in}$ [–]	w_L^{in} [kg/kg]	T_L^{in} [°C]	T_V^{in} [°C]
NH_3/[bmim][BF_4]	29.09	0.030	56	10
NH_3/[emim][SCN]	34.34	0.059	56	10
NH_3/[emim][Tf_2N]	55.92	0.031	56	10
$NH_3/LiNO_3$	3.64	0.374	56	10

[a] Boundary conditions are determined based on a heat pump cycle with operation conditions of $T_{gen}/T_{con}/T_{abs}/T_{eva}$ = 120/45/45/10 °C. The method can be referred to Wang and Infante Ferreira [54]. VLE properties of the IL-based fluids can be found in Wang et al. [53]. It is assumed that the temperature pinch of the solution heat exchanger is 11 K, which is related to the solution inlet condition. The subcooling degrees at the solution inlet are 8.5, 2.8, 1.4 and 25.3 K for the four fluids. The coefficient of performance (for heating) of absorption heat pumps with these fluids are estimated as around 1.6.

Changes of NH_3 mass fraction in the interface and bulk solution for the 3 studied ILs cases along with the reference case are illustrated in Fig. 11.

The levels of interface NH_3 fractions reflect the ILs' solubilities of NH_3. The case with NH_3/[emim][SCN] shows the highest level of NH_3 solubility among the three ILs cases, as expected in previous discussion [54,53]. The fraction differences between the interface and the bulk solution are related to the mass transfer potentials during NH_3 absorption. As indicated, the fluid NH_3/[emim][Tf_2N] provides the least difference and NH_3/[bmim][BF_4] shows a quite large one. Compared with the ILs cases, the $NH_3/LiNO_3$ case has the highest level of NH_3 fractions. Because it has a lower solution flow, the increase of NH_3 fraction in solution of the $NH_3/LiNO_3$ case is also larger than that of the NH_3/ILs cases.

5.2. Overall performance

Parameters concerning the heat transfer, mass transfer and pressure drop are summarized to evaluate the overall performance of the studied fluids in the PHX absorber.

The term $\dot{Q}/A$ is the heat transfer flux across the plate. Using the logarithmic mean temperature difference, *LMTD*, defined in Eq. (10), the overall heat transfer coefficient, *U*, can be obtained to evaluate the heat transfer performance of different fluids in the studied PHX.

$$LMTD = \frac{(T_{L,out} - T_{cw,in}) - (T_{L,in} - T_{cw,out})}{\ln[(T_{L,out} - T_{cw,in})/(T_{L,in} - T_{cw,out})]} \tag{10}$$

$$U = \frac{\dot{Q}/A}{LMTD} \tag{11}$$

However, an application of the *LMTD*, which is only making use of the temperature values in the inlet and outlet of the solution and cooling water streams, may neglect the influence of obvious segments of temperature change, for instance the solution temperature change in this study. Considering it, an integrated averaged temperature difference between the solution and cooling water streams in each control volume, ΔT_{ave}, is used as an alternative to evaluate the overall temperature difference, as defined in Eq. (12). The corresponding overall heat transfer coefficient, U', as provided in Eq. (13) is considered as well.

$$\Delta T_{ave} = \frac{1}{L}\int \Delta T \cdot dL \tag{12}$$

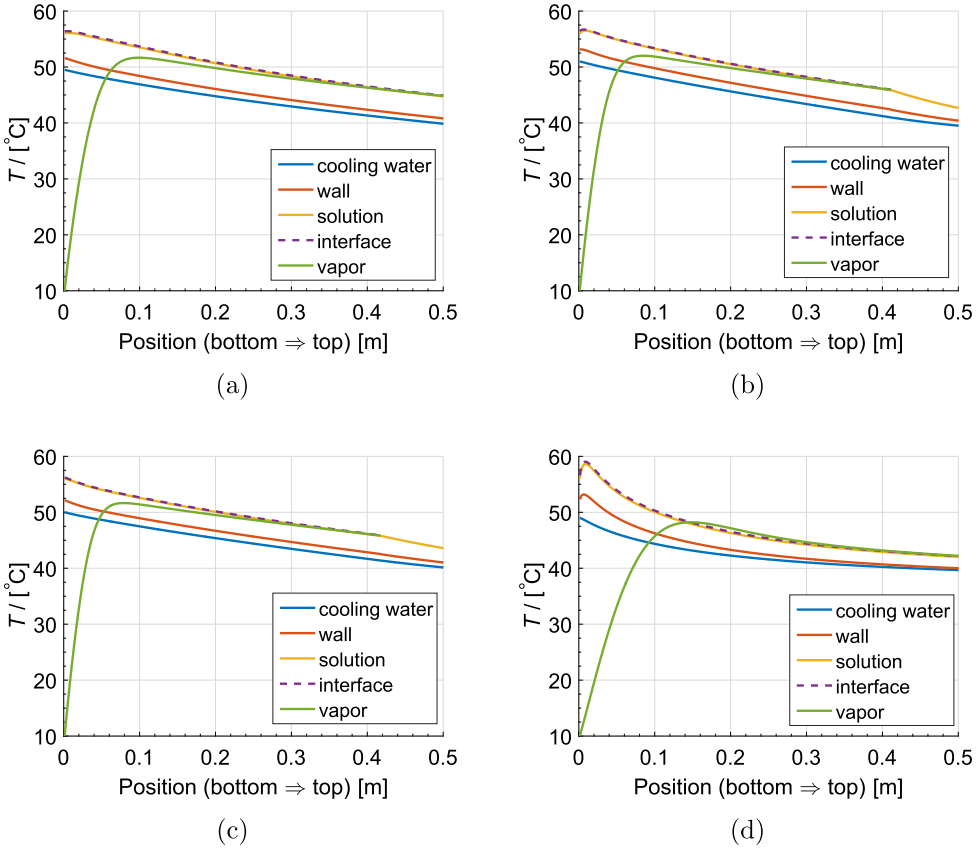

Fig. 10. Temperatures distributions of the studied absorption cases: (a) NH_3/[bmim][BF_4] case, (b) NH_3/[emim][SCN] case, (c) NH_3/[emim][Tf_2N] case, and (d) NH_3/$LiNO_3$ case.

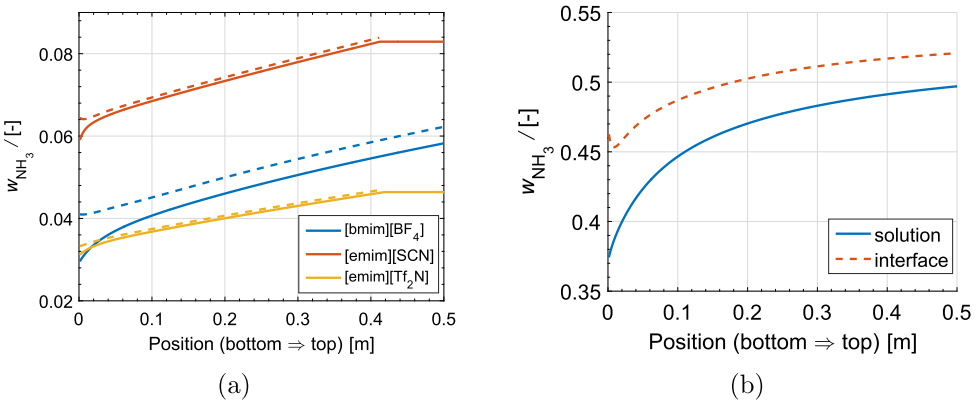

Fig. 11. NH_3 mass fraction distributions of the studied absorption cases: (a) NH_3/ILs cases (dashed curves: interface properties), (b) NH_3/$LiNO_3$ case.

$$U' = \frac{\dot{Q}/A}{\Delta T_{ave}} \tag{13}$$

As for the mass transfer, the term, A_{mt}/A, quantifies the ratio of the effective mass transfer area to the total one. $\dot{G}$ provides the mass flux in the quantified mass transfer area. Subcooling degree of the solution at the outlet, defined as Eq. (14), indicates the mass transfer potential for the solution stream at the outlet.

$$\Delta T^{sub}_{L,out} = T^{sat}_{L}(P_{out,w_{out}}) - T_{L,out} \tag{14}$$

Results of these parameters are obtained and listed in Table 10.

To achieve the same amount of NH_3 absorption with the same cooling medium, the studied cases show more or less similar heat transfer fluxes, $\dot{Q}/A$, which is around 6 kW/m^2. For this specific operating condition, NH_3/[emim][SCN] solution shows the best heat transfer performance among the IL-based fluids. Using the *LMTD* for a rating, it reaches an overall heat transfer coefficient of 1550 W/(m^2·K). The alternative overall heat transfer coefficient, U' is around 1400 W/(m^2·K), which is still the highest among the fluids. NH_3/[emim][SCN] also allows for a promising mass transfer performance. The effective mass transfer area, A_{mt}, takes 83% of the total heat transfer area.

The heat transfer and mass performance of NH_3/[emim][Tf_2N] for the NH_3 absorption comes similar to that of the NH_3/[emim][SCN]. Note that the plate areas in these two fluids cases are not fully used for the vapor absorption. It indicates that there is still

Table 10
Comparison of results on heat transfer, mass transfer and pressure drop of the studied four working fluids in the PHX absorber, in the operating condition of T_{cw}^{in} = 40 °C, $\dot{m}_{cw}$ = 1.41 × 10^{-2} kg/s, and $\dot{m}_{v}$ = 3.89 × 10^{-4} kg/s.

Absorbent		[bmim][BF_4]	[emim][SCN]	[emim][Tf_2N]	$LiNO_3$
$\dot{Q}/A$	[kW/(m^2)]	5.65	6.74	5.77	5.45
LMTD	[K]	5.78	4.34	4.61	4.26
U	[W/(m^2·K)]	977	1552	1253	1280
ΔT_{ave}	[K]	5.77	4.83	4.66	4.27
U′	[W/(m^2·K)]	980	1396	1238	1275
A_{mt}/A	[–]	1	0.83	0.84	1
$\dot{G}$	[×10^{-3} kg/(m^2·s)]	3.44	4.71	4.64	3.46
$\Delta T_{L,out}^{sub}$	[K]	1.88	3.69	2.69	5.74
P_{out}	[kPa]	613.4	615.0	615.0	613.1

room to enhance the mass transfer duty at working fluids side. A discussion of operation conditions in the working fluid side is presented in Section 6.2 based on a sensitivity analysis.

The fluid NH_3/[bmim][BF_4] presents the lowest heat transfer performance of over 970 W/(m^2·K), because of its unfavorable transport properties. For the studied absorption condition, the area of the proposed PHX is not enough to accomplish the gas absorption duty. Nevertheless, the subcooling degree, ΔT_{sub}, of the fluid in the solution outlet is 1.88 K, which indicates it still has sufficient margin for the NH_3 absorption.

The reference fluid, $NH_3/LiNO_3$ shows similar heat transfer performance as the best NH_3/IL fluids. However, the provided area is not sufficient to accomplish the vapor absorption.

For a closer examination of the absorption performance of NH_3 with different working fluids, typical thermophysical properties, parameters related to heat and mass transfer, and relevant dimensionless numbers of the solution stream at the middle position of PHXs are listed in Table 11.

Since the interface heat transfer coefficient cannot be measured directly, the heat and mass transfer analogy is here used to confirm the obtained transfer coefficients are reasonable. The mass transfer coefficient for the $NH_3/LiNO_3$ cases is 1.39 × 10^{-4} m/s. For a similar mass transfer problem (liquid-phase-controlled case) reported by Olujić and Seibert [40], the liquid phase mass transfer coefficients of structured packing, which applies thin corrugated metal plates sharing similar features as the plates in the studied plate heat exchanger, are of the same magnitude as the ones reported in this work. Besides, liquid mass transfer coefficients from H_2O vapor into a falling film of H_2O/LiBr along a vertical tube reported by Miller and Keyhani [38] are also in a similar range. These studies confirm the reasonable prediction of mass transfer coefficient, and consequently, through the heat and mass transfer analogy, confirm the reasonable prediction of the heat transfer coefficients.

The values of mass transfer coefficients, β, for the proposed IL-based fluids are higher than the one for the fluid $NH_3/LiNO_3$. This can be expected since the mass diffusivity, *D*, of the new proposed fluids is 2.4 times to 12 times larger than the mass diffusivity for the $NH_3/LiNO_3$ mixture (0.74 × 10^{-9} m^2/s). Notice that the mass diffusivity of the mixture NH_3/[emim][Tf_2N], which is one of the highest, has been obtained from experiments, see Fig. 9(a). The higher mass diffusivity of ILs-based mixture could be explained by the differences of molecule sizes and structures between the gas and the IL-based solvent which are obviously greater than those between gas and $LiNO_3$. Additionally, the higher mass diffusivity of IL-based mixture has also been reported by Chen et al. [17] which they measured and obtained significantly higher mass diffusivities of H_2O in the mixture H_2O/[mmim][DMP] than in the mixture H_2O/LiBr.

The fluids NH_3/[bmim][BF_4] and NH_3/[emim][SCN] share similar operating conditions of the absorber in heat pump cycles. Most of the thermophysical properties are also quite close, except for their viscosities and mass diffusivities. Even though the relatively higher viscosity can lead to a higher *Pr* ($\propto \mu^{0.33}$), its impact on Reynolds numbers is more dominant in the Nusselt numbers

Table 11
Comparison of relevant thermophysical properties and dimensionless numbers in the middle position of the PHX.

Absorbent		[bmim][BF_4]	[emim][SCN]	[emim][Tf_2N]	$LiNO_3$
T	[°C]	49.4	49.3	49.0	45.1
P	[kPa]	614.3	615.1	615.1	614.2
w	[kg/kg]	0.048	0.076	0.042	0.478
ρ	[kg/m^3]	1154	1061	1456	1003
c_p	[J/(kg·K)]	1823	1972	1484	3084
λ	[mW/(m·K)]	194	226	132	301
D	[×10^{-9} m^2/s]	1.75	8.63	5.82	0.74
μ	[×10^{-3} Pa·s]	3.39	1.42	1.28	4.60
σ	[×10^{-2} N/m]	4.08	4.84	3.38	5.20
δ_f	[×10^{-4} m]	7.96	8.44	8.73	2.86
α_{Lw}	[W/(m^2·K)]	1219	2010	1699	1287
α_{Lint}	[W/(m^2·K)]	18553	41273	39366	11113
β	[×10^{-4} m/s]	6.28	36.61	37.91	1.39
Nu_{Lw}	[–]	4.99	7.52	11.20	1.22
Nu_{Lint}	[–]	75.98	154.39	259.49	10.56
Pr	[–]	31.76 (52[a])	12.38 (15[a])	14.40 (18[a])	47.09 (80[a])
Sh	[–]	284.77	358.30	568.66	53.71
Sc	[–]	1672 (2265[a])	155 (175[a])	152 (172[a])	6190 (10649[a])

[a] Solution Prandtl or Schmidt numbers at the entrance of PHX are shown inside brackets. They, together with the entrance Reynolds numbers as shown in Fig. 12, are used to quantify the solution Nusselt and Sherwood number, respectively.

($\propto \mu^{-0.6139}$ and $\propto \mu^{-0.8381}$), which leads to a worse heat transfer performance. Together with the relatively lower mass diffusivity of NH_3/[bmim][BF_4], its heat and mass transfer performance is not promising.

The fluid NH_3/[emim][SCN] has similar values of *Pr* and *Sc* with those of the NH_3/[emim][Tf_2N] fluid. It implies that these two fluids share comparable ratios of thermal and mass diffusivities to the viscous diffusivity. However, the large solution flow for the fluid NH_3/[emim][Tf_2N] (see Table 9) leads to a large Re_L, and hence the flow convection promotes heat and mass transfer. Note that the large flow also requires a significant consumption of pump work, which is not negligible in large pressure drop applications, for instance the double-effect cycle discussed in Wang et al. [53]. The selection of ILs for the absorption system requires a trade-off between operational and initial costs.

6. Discussions

6.1. Validations of the proposed flow patterns

The thin film feature of the solution flow inside the PHX has been re-examined in the following two ways for the cases considered in this study.

The work of Tao et al. [44] presents three different maps to distinguish flow patterns of downward condensation and absorption two-phase flow inside PHXs. The recommended one is a pair of dimensionless numbers: Re_L and Fr/Λ^2. Re_L represents flow characteristics of the liquid phase. *Fr* number accounts for the influence of vapor flow. Λ is a correction factor of fluid properties, which is defined as,

$$\Lambda = \frac{\mu_L/\mu_{H_2O}}{\left[\frac{\rho_L}{\rho_{H_2O}}\left(\frac{\sigma_L}{\sigma_{H_2O}}\right)^3\right]^{1/4}} \tag{15}$$

Even though the map is not derived for the flow direction studied in this work, these two parameters can however give an indication of the expected vapor and liquid distribution along the flow through the heat exchanger. In Fig. 12, the studied cases are represented inside the map according to the relevant dimensionless numbers.

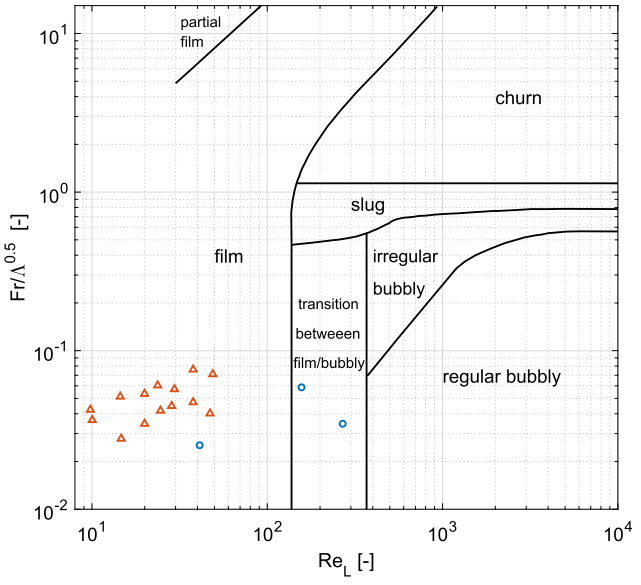

Fig. 12. The studied cases shown in the flow pattern map proposed in Tao et al. [44]. Triangle symbols represent the cases with the fluid NH_3/$LiNO_3$, round ones represent the cases with NH_3/IL fluids.

As shown in Fig. 12, values of Re_L and Fr/Λ^2 of most cases in this study fall into the film flow region. Only for the fluid NH_3/[emim][Tf_2N], the flow may transit from film to bubbly region, this is mainly due to the large liquid flow required.

The other examination is carried out by assuming a bubble flow is dominant for the investigated cases.

Fig. 13 shows visualization results of flow patterns in NH_3/$LiNO_3$ vertical tubular absorbers with cocurrent upward flows of liquid and vapor phases reported by Infante Ferreira [27].

As the flow passage area reduces from right (diameter = 25 mm) to left (diameter = 10 mm), the vapor slugs become longer and a thin film of solution is formed between the slug and the wall. The authors expect that, with an even narrower flow passage area in plate heat exchangers, the vapour slugs become even longer so that film flow is predominant in the absorber.

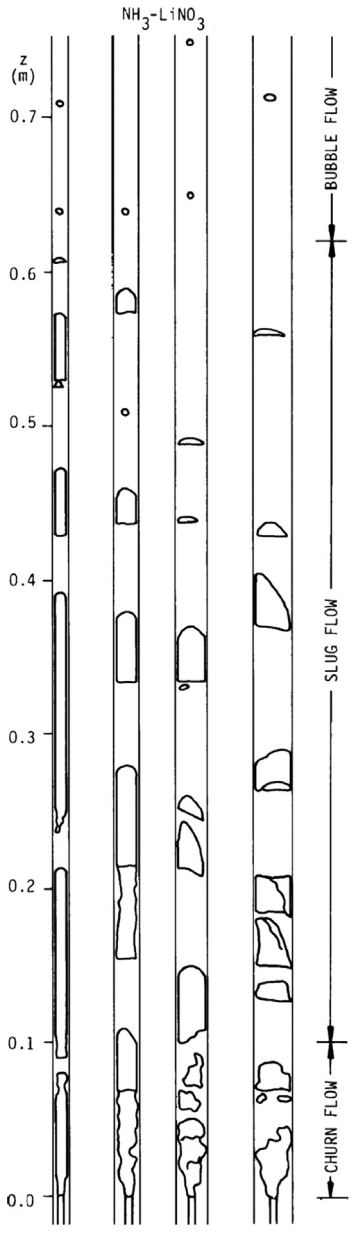

Fig. 13. Visualizations of flow patterns in NH_3/$LiNO_3$ vertical tubular absorbers with cocurrent upward flows [27]. The ammonia vapor flow is in average 72.5×10^{-6} kg/s, the solution flow 5.5×10^{-3} kg/s.

Furthermore, diameters of initial bubbles leaving the orifice can also be estimated based on equations provided by Treybal [47]. Considering an orifice of 1 mm diameter, the orifice Reynolds numbers, Re_{ori},

$$Re_{ori} = \frac{d_{ori} \cdot v_{ori} \cdot \rho_V}{\mu_V} \tag{16}$$

which are based on the vapor velocity through the orifice and the orifice diameter as the characteristic length, show values larger than 10^5 for the studied cases.

It indicates that the selected gas rate in simulations and also the NH_3/$LiNO_3$ experimental conditions all have large vapor velocities through the orifice. The corresponding estimation of initial bubble diameters is provided by Eq. (17), which is only related to the NH_3 vapor flow.

$$d_{ini} = 0.0071 \cdot Re_{ori}^{-0.05} \tag{17}$$

For the studied NH_3/$LiNO_3$ cases, the values of initial bubble diameters are in the range of 4.0–4.7 mm. For all the NH_3/ILs cases, the initial bubble diameters are 4.0 mm identically.

The estimated initial bubble diameters of these cases are all larger than the gap between plates (2 mm), which implies a deformed bubble would pass through the channel. These facts indicate that the assumption of a thin film flow for the solution stream is sufficient accurate to represent the physics of the liquid phase of vapor-liquid absorption inside the PHX.

6.2. Sensitivity analysis of transport properties and operation conditions

The availability of transport properties for NH_3-IL mixtures is limited. The current property method, which is based on very few reported property data may introduce errors on the overall heat and mass transfer calculation. Here a sensitivity analysis is carried out to investigate the influence of the uncertainty of two fundamental transport properties, mass diffusivity of NH_3 into the NH_3/IL mixture and viscosities of the mixture, on the heat and mass transfer performance estimated by the proposed framework.

Fig. 14 illustrates an evaluation of scaled properties on the two overall heat transfer coefficients (U and U'), mass transfer flux on the effective mass transfer area ($\dot{G}$) and the area ratio of the plates needed for mass transfer (A_{mt}) for the working pair NH_3/[emim][Tf_2N]. The operating conditions are the same as introduced in Section 5.

A lower value of mass diffusivity has a limited influence on the heat transfer as shown in Fig. 14(a). It mainly affects the mass transfer. A 90% decrease of D (maximum deviation) can introduce a drop of mass transfer coefficient of 18%. In that case, the current PHX can not complete the mass transfer duty. Notice that the experimental data is predicted in average with a deviation smaller than −50%. For such decrease, the reduction of the mass transfer flux is only around 5%.

The current method used to predict the mixture viscosity may underestimate it for a real solution. As the method may introduce an average error of −50%, it can cause a 12–20% decrease of overall heat transfer coefficients and a 15% decrease of the mass transfer flux. For an extreme case when the mixture viscosity is 10 times larger than the predicted one, heat and mass transfer will be deteriorated significantly. In that case, overall heat transfer performance and total mass transfer flux both drop 40%.

Moreover, operating conditions in the working fluid side, the solution inlet temperature, T_L^{in}, and the flow, $\dot{m}_V$, are also studied to evaluate their influences on the heat and mass transfer performance, as presented in Fig. 15. Notice that except for the studied variable, other operating conditions are the same as introduced in Section 5, including the ratio of $\dot{m}_L$ to $\dot{m}_V$.

As shown in Fig. 15(a), a lower inlet solution temperature can enhance the NH_3 absorption, thus the mass transfer flux improves and the area needed for mass transfer decreases. The heat duty is reduced at lower T_L^{in} cases, causing the overall heat transfer coefficient, U', predicted using Eqs. (12) and (13), to drop. The deviation of its behavior from the standard overall heat transfer coefficient, U, estimated using Eqs. (10) and (11), is due to the large temperature rise at the inlet of working fluids, which is a result of a larger amount of absorption heat released.

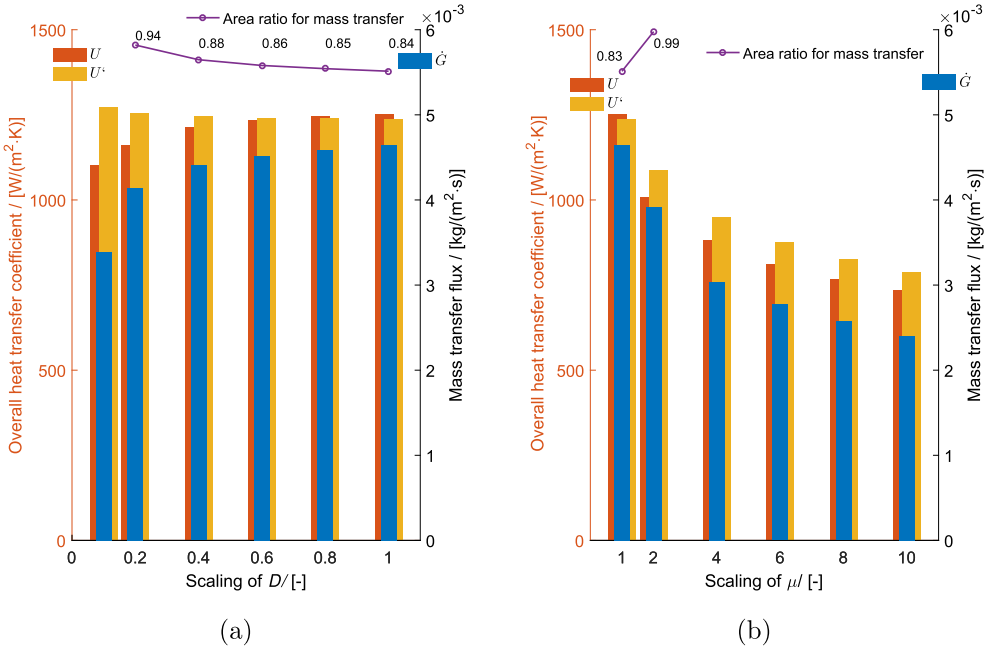

Fig. 14. Sensitivity analysis of (a) mass diffusivity and (b) mixture viscosity on the overall heat and mass transfer performance of NH_3's absorption into NH_3/[emim][Tf_2N] solution.

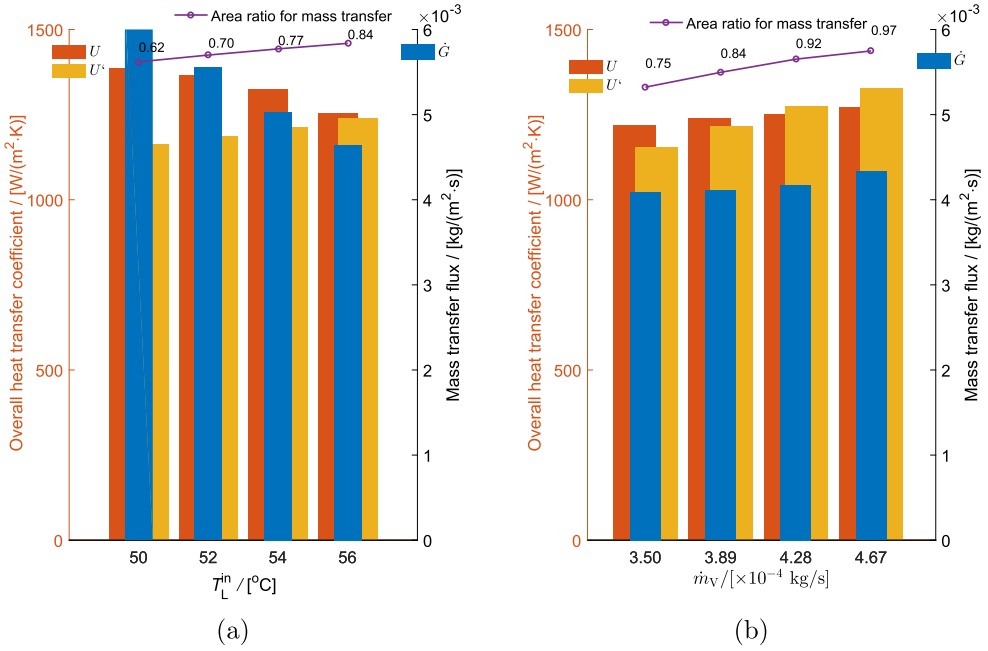

Fig. 15. Sensitivity analysis of (a) solution inlet temperature and (b) vapor flow rate on the overall heat and mass transfer performance of NH_3's absorption into NH_3/[emim][Tf_2N] solution.

Fig. 15(b) shows that an increase of the working fluid flows can enhance both the heat and mass transfer performance. At the best design point when the vapor flow, $\dot{m}_V$, is 4.67×10^{-4} kg/s, the current PHX is almost fully used for the absorption duty.

7. Conclusions

This work aims at providing knowledge on the absorber design for IL-based absorption systems. A semi-empirical framework is proposed to study the heat and mass transfer during the absorption of NH_3 into NH_3/non-volatile salts solutions inside corrugated plate heat exchangers. Experimental data of $NH_3/LiNO_3$ absorption is applied to determine unknown information concerning the heat and mass transfer performance of the solution film. The identified relations are then used in combination with the thermophysical data of NH_3/ILs, to predict the performance of the absorber of an NH_3/ILs absorption heat pump cycle.

- The friction factors of the $NH_3/LiNO_3$ absorption in the studied PHX have been correlated as a function of solution Reynolds number: $\xi = 23050 \cdot Re_L^{-1.69}$.
- Nusselt numbers of the liquid film to the wall and interface are determined, showing relations with the solution Reynolds number: $Nu_{L,w} = 0.1372 \cdot Re_L^{0.6139} \cdot Pr^{1/3}$, and $Nu_{L,int} = 0.9077 \cdot Re_L^{0.8381} \cdot Pr^{1/3}$. The Nusselt number of the liquid film at the interface side is much larger than the one at the wall side.
- A stronger absorption is detected in the entrance of the absorber, which may cause a rapid temperature rise.
- The effective mass diffusivity of NH_3 in ILs is proposed as an exponential relation to the pure IL's viscosity with an exponent of -1.45.
- The ranking of the heat transfer performance for the NH_3/ILs is: [emim][SCN] > [emim][Tf_2N] > [bmim][BF_4]. An absorber with the studied geometry can achieve an overall heat transfer coefficient of 1.4 kW/(m^2K) under the studied condition, which is comparable with the performance of $NH_3/LiNO_3$'s absorber.
- The averaged uncertainties of the mass diffusitivity and viscosity predicted using the current property methods will cause less than 20% reductions to the overall heat and mass transfer performance under the studied conditions.

Declarations of interest

None.

Acknowledgment

The authors would like to acknowledge the financial support from the China Scholarship Council (Scholarship 201406320184). LH acknowledges financial support provided by the National Natural Science Foundation of China (NSFC) (Grant No. 51106068 and 51566014) and the Foundation for Returnees of Inner Mongolia.

Appendix A. Supplementary material

Supplementary data associated with this article can be found, in the online version, at https://doi.org/10.1016/j.ijheatmasstransfer.2019.02.063.

References

[1] E.-S. Abumandour, F. Mutelet, D. Alonso, Performance of an absorption heat transformer using new working binary systems composed of {ionic liquid and water}, Appl. Therm. Eng. 94 (2016) 579–589.
[2] H.F.D. Almeida, A.R.R. Teles, J.A. Lopes-Da-Silva, M.G. Freire, J.A.P. Coutinho, Influence of the anion on the surface tension of 1-ethyl-3-methylimidazolium-based ionic liquids, J. Chem. Thermodyn. 54 (2012) 49–54.
[3] C.F. Amaris Castilla, Intensification of NH3 Bubble Absorption Process using Advanced Surfaces and Carbon Nanotubes for $NH_3/LINO_3$ Absorption Chillers (Ph.D. thesis), Universitat Rovira i Virgili, 2013.
[4] H.M. Ariyadi, A. Cera-Manjarres, A. Coronas, Absorption behaviour and diffusivity of ammonia in ionic liquids, in: 5th IIR International Conference on Thermophysical Properties and Transfer Processes of Refrigerants, 2017.
[5] H.M. Ariyadi, A. Coronas, Absorption capacity of ammonia into ionic liquids for absorption refrigeration applications, J. Phys: Conf. Ser. 745 (2016) 032105.
[6] D.S. Ayou, M.R. Currás, D. Salavera, J. García, J.C. Bruno, A. Coronas, Performance analysis of absorption heat transformer cycles using ionic liquids based on imidazolium cation as absorbents with 2,2,2-trifluoroethanol as refrigerant, Energy Convers. Manage. 84 (2014) 512–523.
[7] J. Bedia, J. Palomar, M. Gonzalez-Miquel, F. Rodriguez, J.J. Rodriguez, Screening ionic liquids as suitable ammonia absorbents on the basis of thermodynamic and kinetic analysis, Sep. Purif. Technol. 95 (2012) 188–195.

[8] T.L. Bergman, A.S. Lavine, F.P. Incropera, D.P. Dewitt, Fundamentals of Heat and Mass Transfer, John Wiley & Sons, Inc., 2011.
[9] R.B. Bird, W.E. Stewart, E.N. Lightfoot, Transport Phenomena, Wiley International ed., Wiley, 2007.
[10] D.B. Boman, D.C. Hoysall, M.A. Staedter, A. Goyal, M.J. Ponkala, S. Garimella, A method for comparison of absorption heat pump working pairs, Int. J. Refrig. 77 (2017) 149–175.
[11] N. Brauner, Non-isothermal vapour absorption into falling film, Int. J. Heat Mass Transfer 34 (3) (1991) 767–784.
[12] W. Cai, M. Sen, S. Paolucci, Dynamic modeling of an absorption refrigeration system using ionic liquids, in: Volume 6: Energy Systems: Analysis, Thermodynamics and Sustainability, ASME, Seattle, 2007, pp. 227–236.
[13] A. Cera-Manjarres, Experimental Determination and Modelling of Thermophysical Properties of Ammonia/ionic Liquid Mixtures for Absorption Refrigeration Systems (Ph.D. thesis), Universitat Rovira i Virgili, 2015.
[14] J. Cerezo, R. Best, M. Bourouis, A. Coronas, Comparison of numerical and experimental performance criteria of an ammonia–water bubble absorber using plate heat exchangers, Int. J. Heat Mass Transfer 53 (17–18) (2010) 3379–3386.
[15] J. Cerezo, R. Best, R. Romero, A study of a bubble absorber using a plate heat exchanger with NH_3–H_2O, NH_3–$LiNO_3$ and NH_3–NaSCN, Appl. Therm. Eng. 31 (11–12) (2011) 1869–1876.
[16] J. Cerezo, M. Bourouis, M. Vallès, A. Coronas, R. Best, Experimental study of an ammonia-water bubble absorber using a plate heat exchanger for absorption refrigeration machines, Appl. Therm. Eng. 29 (5–6) (2009) 1005–1011.
[17] W. Chen, B. Zhang, Z. Liu, M. Zhao, Z. Miao, Investigation of the mutual diffusion coefficients of [mmim]DMP/H_2O and [mmim]DMP/CH_3OH at atmospheric pressure, Int. J. Heat Mass Transfer 111 (2017) 559–569.
[18] Y. Cuenca, D. Salavera, A. Vernet, A.S. Teja, M. Vallès, Thermal conductivity of ammonia + lithium nitrate and ammonia + lithium nitrate + water solutions over a wide range of concentrations and temperatures, Int. J. Refrig. 38 (1) (2014) 333–340.
[19] L. Dong, D. Zheng, N. Nie, Y. Li, Performance prediction of absorption refrigeration cycle based on the measurements of vapor pressure and heat capacity of H_2O+[DMIM]DMP system, Appl. Energy 98 (2012) 326–332.
[20] L.E. Ficke, R.R. Novak, J.F. Brennecke, Thermodynamic and thermophysical properties of ionic liquid + water systems, J. Chem. Eng. Data 55 (11) (2010) 4946–4950.
[21] A.P. Fröba, M.H. Rausch, K. Krzeminski, D. Assenbaum, P. Wasserscheid, A. Leipertz, Thermal conductivity of ionic liquids: measurement and prediction, Int. J. Thermophys. 31 (11–12) (2010) 2059–2077.
[22] J. Gao, N.J. Wagner, Non-ideal viscosity and excess molar volume of mixtures of 1-butyl-3-methylimidazolium tetrafluoroborate ($[C_4mim][BF_4]$) with water, J. Mol. Liq. 223 (2016) 678–686.
[23] M.H. Ghatee, A.R. Zolghadr, Surface tension measurements of imidazolium-based ionic liquids at liquid-vapor equilibrium, Fluid Phase Equilib. 263 (2) (2008) 168–175.
[24] G. Grossman, Simultaneous heat and mass transfer in film absorption under laminar flow, Int. J. Heat Mass Transfer 26 (3) (1983) 357–371.
[25] A. Hofmann, M. Migeot, T. Hanemann, Investigation of binary mixtures containing 1-ethyl-3-methylimidazolium bis(trifluoromethanesulfonyl) azanide and ethylene carbonate, J. Chem. Eng. Data 61 (1) (2016) 114–123.
[26] C. Infante Ferreira, Thermodynamic and physical property data equations for ammonia-lithium nitrate and ammonia-sodium thiocyanate solutions, Sol. Energy 32 (2) (1984) 231–236.
[27] C.A. Infante Ferreira, Vertical Tubular Absorbers for Ammonia-salt Absorption Refrigeration (Ph.D. thesis), Delft University of Technology, 1985.
[28] T. Jin, M. Wang, K. Tang, Simulation and performance analysis of a heat transfer tube in SuperORV, Cryogenics 61 (2014) 127–132.
[29] Y.T. Kang, A. Akisawa, T. Kashiwagi, Analytical investigation of two different absorption modes, Int. J. Refrig. 23 (6) (2000) 430–443.
[30] S. Kim, Y.J. Kim, Y.K. Joshi, A.G. Fedorov, P.A. Kohl, Absorption heat pump/refrigeration system utilizing ionic liquid and hydrofluorocarbon refrigerants, J. Electron. Packag. 134 (3) (2012) 031009.
[31] E.W. Lemmon, M.L. Huber, M.O. McLinden, NIST reference fluid thermodynamic and transport properties–REFPROP, 2013.
[32] S. Libotean, A. Martín, D. Salavera, M. Valles, X. Esteve, A. Coronas, Densities, viscosities, and heat capacities of ammonia + lithium nitrate and ammonia + lithium nitrate + water solutions between (293.15 and 353.15) K, J. Chem. Eng. Data 53 (10) (2008) 2383–2388.
[33] S. Libotean, D. Salavera, M. Valles, X. Esteve, A. Coronas, Vapor-liquid equilibrium of ammonia + lithium nitrate + water and ammonia + lithium nitrate solutions from (293.15 to 353.15) K, J. Chem. Eng. Data 52 (3) (2007) 1050–1055.
[34] N. Merkel, M. Bücherl, M. Zimmermann, V. Wagner, K. Schaber, Operation of an absorption heat transformer using water/ionic liquid as working fluid, Appl. Therm. Eng. 131 (2018) 370–380.
[35] T. Meyer, R. Kühn, C. Ricart, T. Zegenhagen, F. Ziegler, Simulation of an absorption refrigerator working with ionic liquids and natural refrigerants, in: Proceedings of the 24th IIR International Congress of Refrigeration. Yokohama, Japan, Paper ID: 895, 2015.
[36] T. Meyer, M. Winker, S. Bergemann, R. Kühn, C. Ricart, F. Ziegler, Experimental investigation of an absorption refrigerator working with ionic liquid and ethanol, in: Proceedings of the 5th IIR International Conference on Thermophysical Properties and Transfer Processes of Refrigerants. Seoul, South Korea, Paper ID: 035, 2017.
[37] B. Michel, N. Le Pierrès, B. Stutz, Performances of grooved plates falling film absorber, Energy 138 (2017) 103–117.
[38] W.A. Miller, M. Keyhani, The correlation of simultaneous heat and mass transfer experimental data for aqueous lithium bromide vertical falling film absorption, J. Sol.Energy Eng. 123 (1) (2001) 30.
[39] D. Morgan, L. Ferguson, P. Scovazzo, Diffusivities of gases in room-temperature ionic liquids: data and correlations obtained using a lag-time technique, Ind. Eng. Chem. Res. 44 (13) (2005) 4815–4823.
[40] Ž. Olujić, A.F. Seibert, Predicting the liquid phase mass transfer resistance of structured packings, Chem. Biochem. Eng. Quart. J. 28 (4) (2014) 409–424.
[41] C. Oronel, C. Amaris, M. Bourouis, M. Vallès, Heat and mass transfer in a bubble plate absorber with $NH_3/LiNO_3$ and $NH_3/(LiNO_3 + H_2O)$ mixtures, Int. J. Therm. Sci. 63 (2013) 105–114.
[42] J. Salgado, T. Regueira, L. Lugo, J. Vijande, J. Fernández, J. García, Density and viscosity of three (2,2,2-trifluoroethanol + 1-butyl-3-methylimidazolium) ionic liquid binary systems, J. Chem. Thermodyn. 70 (2014) 101–110.
[43] M.B. Shiflett, A. Yokozeki, Solubility and diffusivity of hydrofluorocarbons in room-temperature ionic liquids, AIChE J. 52 (3) (2006) 1205–1219.
[44] X. Tao, M.P. Nuijten, C.A. Infante Ferreira, Two-phase vertical downward flow in plate heat exchangers: flow patterns and condensation mechanisms, Int. J. Refrig. 85 (2018) 489–510.
[45] M. Tariq, A.P. Serro, J.L. Mata, B. Saramago, J.M. Esperança, J.N. Canongia Lopes, L.P.N. Rebelo, High-temperature surface tension and density measurements of 1-alkyl-3-methylimidazolium bistriflamide ionic liquids, Fluid Phase Equilib. 294 (1–2) (2010) 131–138.
[46] C.M. Tenney, M. Massel, J.M. Mayes, M. Sen, J.F. Brennecke, E.J. Maginn, A computational and experimental study of the heat transfer properties of nine different ionic liquids, J. Chem. Eng. Data 59 (2) (2014) 391–399.
[47] R.E. Treybal, Mass-transfer Operations, third ed., McGraw-Hill Inc, 1980.
[48] D. Triché, S. Bonnot, M. Perier-Muzet, F. Boudéhenn, H. Demasles, N. Caney, Experimental and numerical study of a falling film absorber in an ammonia-water absorption chiller, Int. J. Heat Mass Transfer 111 (2017) 374–385.
[49] M.E.V. Valkenburg, R.L. Vaughn, M. Williams, J.S. Wilkes, Thermochemistry of ionic liquid heat-transfer fluids, Thermochim. Acta 425 (1–2) (2005) 181–188.
[50] M. Venegas, M. Izquierdo, P. Rodríguez, A. Lecuona, Heat and mass transfer during absorption of ammonia vapour by $LiNO_3$–NH_3 solution droplets, Int. J. Heat Mass Transfer 47 (12–13) (2004) 2653–2667.
[51] V.V. Wadekar, Ionic liquids as heat transfer fluids – an assessment using industrial exchanger geometries, Appl. Therm. Eng. 111 (2017) 1581–1587.
[52] M. Wang, T.M. Becker, C.A. Infante Ferreira, Assessment of vapor–liquid equilibrium models for ionic liquid based working pairs in absorption cycles, Int. J. Refrig. 87 (2018) 10–25.
[53] M. Wang, T.M. Becker, B.A. Schouten, T.J. Vlugt, C.A. Infante Ferreira, Ammonia/ionic liquid based double-effect vapor absorption refrigeration cycles driven by waste heat for cooling in fishing vessels, Energy Convers. Manage. 174 (2018) 824–843.
[54] M. Wang, C.A. Infante Ferreira, Absorption heat pump cycle with NH_3 - ionic liquid working pairs, Appl. Energy 204 (July) (2017) 819–830.
[55] P. Wasserscheid, M. Seiler, Leveraging gigawatt potentials by smart heat-pump technologies using ionic liquids, ChemSusChem 4 (4) (2011) 459–463.
[56] A. Yokozeki, M.B. Shiflett, Ammonia solubilities in room-temperature ionic liquids, Ind. Eng. Chem. Res. 46 (5) (2007) 1605–1610.
[57] A. Yokozeki, M.B. Shiflett, Vapor–liquid equilibria of ammonia+ionic liquid mixtures, Appl. Energy 84 (12) (2007) 1258–1273.
[58] D. Zheng, L. Dong, W. Huang, X. Wu, N. Nie, A review of imidazolium ionic liquids research and development towards working pair of absorption cycle, Renew. Sustain. Energy Rev. 37 (2014) 47–68.
[59] S.M. Zivi, Estimation of steady-state steam void-fraction by means of the principle of minimum entropy production, J. Heat Transfer 86 (2) (1964) 247–251.